

Cite this: *Dalton Trans.*, 2023, **52**, 1720

# Iron complexes of bridging azo ligands in aqueous solution: changes in the thermal switching mechanism on coordination and oxidation state of metal centres†

Manuel Bardají,<sup>a</sup> Mercè Font-Bardia,<sup>b</sup> Albert Gallen,<sup>c</sup> Beltzane Garcia-Cirera,<sup>c</sup> Montserrat Ferrer<sup>\*c,d</sup> and Manuel Martínez<sup>ID \*c,d</sup>

Three azobenzenes  $\text{CN}(\text{C}_6\text{H}_4)\text{-N}=\text{N}(\text{-C}_5\text{H}_4\text{N})$  (**py-iso**),  $\text{CN}(\text{C}_6\text{H}_4)\text{-N}=\text{N}(\text{-C}_6\text{H}_4)\text{CN}$  (**cyano-iso**) and  $\text{CN}(\text{C}_6\text{H}_4)\text{-N}=\text{N}(\text{-C}_6\text{H}_4)\text{NC}$  (**iso-iso**) with good coordinating groups (pyridine, phenylcyano or phenylisocyanato) at the ends of the diazenyl unit have been synthesized and fully characterised. These compounds have been used as ligands in the synthesis of water-soluble metallic species by coordination to  $\{\text{Fe}^{\text{II}}(\text{CN})_5^{3-}\}$  units, either in one or two of the anchoring groups of the derivatives. Both the azo derivatives and their complexes are photochemically active with respect to their *trans*-to-*cis* isomerisation process. Their *cis*-to-*trans* reverse thermal reaction has been thoroughly studied as a function of the donor groups, solvent, temperature and pressure, in order to gain insight into the rotation or inversion mechanisms involved in the process. A comparison of the isomerisation mechanism between the iron complexes and the corresponding free ligands revealed an interesting fine tuning of the process on coordination of the  $\{\text{Fe}^{\text{II}}(\text{CN})_5^{3-}\}$  moieties, which may even produce, in some cases, non-photoswitchable species containing typically photoactive units.

Received 24th November 2022,  
Accepted 20th December 2022

DOI: 10.1039/d2dt03790d

rsc.li/dalton

## Introduction

Azobenzene derivatives are historical compounds that exhibit reversible and robust photochemical isomerisation reactions around their central diazene unit (Scheme 1).<sup>1</sup> There are many studies dealing with these photochemical processes, both occurring at high energies (producing the *cis* isomer from the

*trans* thermodynamically stable form) as well as the lower energy back reaction; these have been comprehensively studied and reviewed.<sup>2</sup>

The complementary back *cis*-to-*trans* thermal isomerisation reaction has also been thoroughly studied, given the importance of the process involved in photoswitching materials.<sup>3,4</sup> The thermal process has been found dependent on a wealth of factors that, ultimately, relate to structural characteristics that favour rotation (charge-separated) or inversion (non-charge-separated) transition states.<sup>5,6</sup> These characteristics have been mostly tuned by push-pull functionalisation of the diazene-containing molecule in order to achieve a desired switching response time.<sup>7</sup> Nevertheless, the choice of solvent has also been found to be crucial for the establishment of the isomeri-

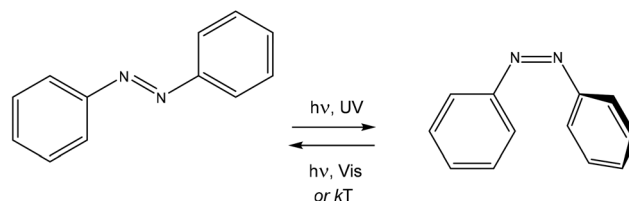
<sup>a</sup>IU CINQUIMA/Química Inorgánica, Facultad de Ciencias, Universidad de Valladolid, 47071 Valladolid, Spain

<sup>b</sup>Unitat de Difracció de RX, Centres Científics i Tecnològics de la Universitat de Barcelona (CCiTUB). Universitat de Barcelona, Solé i Sabarís 1-3, 08028 Barcelona, Spain

<sup>c</sup>Secció de Química Inorgànica, Departament de Química Inorgànica i Orgànica, Universitat de Barcelona, Martí i Franquès 1-11, 08028 Barcelona, Spain.  
E-mail: montse.ferrer@qi.ub.edu, manel.martinez@qi.ub.edu

<sup>d</sup>Institute of Nanoscience and Nanotechnology (IN2UB), Universitat de Barcelona, 08028 Barcelona, Spain

† Electronic supplementary information (ESI) available: Experimental procedures for the preparation and characterisation of the azo ligands. Observed rate constants for the thermal *cis*-to-*trans* spontaneous process of the iron derivatives studied as a function of the different variables. Observed rate constants for the peroxodisulfate oxidation of the  $\text{Na}_3[(\text{NC})_5\text{Fe}^{\text{II}}\text{CN}(\text{C}_6\text{H}_4)\text{-N}=\text{N}(\text{-C}_5\text{H}_4\text{N})]$  complex as a function of the different variables. CCDC 2216961. For ESI and crystallographic data in CIF or other electronic format see DOI: <https://doi.org/10.1039/d2dt03790d>

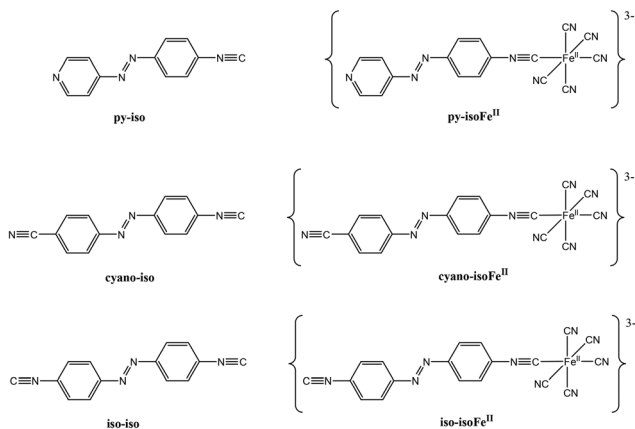


Scheme 1 Isomerisation processes in azobenzene derivatives.

sation mechanism underlying the process.<sup>8</sup> In all cases, the comprehensive solvent, temperature and pressure dependence of the isomerisation kinetics, including the determination of the thermal ( $\Delta H^\ddagger$  and  $\Delta S^\ddagger$ ) and pressure ( $\Delta V^\ddagger$ ) activation parameters,<sup>9,10</sup> has been found to be an ideal tool for this purpose.<sup>11–13</sup>

The simplest coordination of these compounds to metal centres usually involves the nitrogen donors of the diazene moiety to the metals.<sup>14</sup> These reactions normally produce photochemically inactive mono- and dinuclear-cyclometalated derivatives.<sup>15–20</sup> Nevertheless, functionalisation of the phenyl rings of these derivatives with different donor groups has also been conducted, with the aim of having a photoactive dangling azo moiety coordinatively attached to a transition metal.<sup>21–27</sup> The possible implication of these appended photoswitches in biologically relevant interactions has also been reported.<sup>28,29</sup> Furthermore, the incorporation of derivatives having both phenyl rings modified with suitable donors has also been explored for its inclusion in transition metal 2D and 3D frameworks.<sup>30–34</sup>

In view of the latter, and given our interest in the assembly of discrete mixed valence cyanido-bridged  $\text{Co}^{\text{III}}/\text{Fe}^{\text{II}}$  compounds,<sup>35–42</sup> we decided to explore the incorporation of *para*-isocyanide substituents to azo derivatives for the construction of  $\{\text{Fe}^{\text{II}}(\text{CN})_5(\text{CN-R}_{\text{azoo}})^{3-}\}$  units as photoactive building blocks for the assembly of molecular species of high nuclearity (Scheme 2). The exact determination of their isomerisation mechanisms and solvent dependence has also been established with the aim to ultimately determine the possible photochemical/thermal switching of the cavity size of the structures generated. This is a fact that is extremely relevant, given the importance of the cavity and portal size involved in catalysis, encapsulation, and encapsulation-derived properties of discrete molecular structures.<sup>35,43–45</sup> Furthermore, the hindrance of some thermal *cis*-to-*trans* switching behaviours, due to the rotational mechanisms operating on the assembled structures generated, distinct from the inversion mechanism actuation on the free ligand, also poses a new challenge for the design of such assemblies.



**Scheme 2** Free isocyanide-appended azo derivatives and  $\{\text{Fe}^{\text{II}}(\text{CN})_5(\text{CN-R}_{\text{azoo}})^{3-}\}$  complexes.

## Results and discussion

### Bridging azo ligands

Both the 4-((4-isocyanophenyl)diazanyl)pyridine,  $\text{CN}(\text{C}_6\text{H}_4)\text{-N}=\text{N}(\text{C}_5\text{H}_4\text{N})$  (**py-iso**), and the 4-((4-isocyanophenyl)diazanyl)benzonitrile,  $\text{CN}(\text{C}_6\text{H}_4)\text{-N}=\text{N}(\text{C}_6\text{H}_4)\text{CN}$  (**cyano-iso**), compounds (Scheme 2) have been prepared by the standard condensation of aniline and 4-aminopyridine or 4-aminobenzonitrile with  $\text{NaNO}_2$ .<sup>46</sup> The formation of the amido derivative and its dehydration using phosgene have been conducted, optimising the established method.<sup>22,47,48</sup> The two new compounds have been characterised by  $^1\text{H}$  and  $^{13}\text{C}$  NMR, IR, and UV-Vis spectroscopy and ESI MS, as indicated in the Experimental section; single crystal XRD of  $\text{CN}(\text{C}_6\text{H}_4)\text{-N}=\text{N}(\text{C}_6\text{H}_4)\text{CN}$  has also been conducted and the structure corresponds to the spectroscopic assignment (Fig. S1†). The already reported 4,4'-diisocyanobenzene,  $\text{CN}(\text{C}_6\text{H}_4)\text{-N}=\text{N}(\text{C}_6\text{H}_4)\text{NC}$  (**iso-iso**) (Scheme 2), compound was prepared using similar procedures to those indicated above, and its characterisation agrees with the literature data.<sup>49</sup> Electrochemical experiments were carried out in acetonitrile solutions of all the azo derivatives; two fully reversible signals at  $-60$  and  $-105$  mV (*versus* the SHE) were obtained in all cases, in agreement with the expected data from the literature.<sup>50,51</sup>

As indicated in the Experimental section, the  $^1\text{H}$  NMR spectra of the irradiated solutions at 365 nm feature the set of signals assigned to the *cis* isomers apart from the major *trans* isomeric thermally dominant form. Thus, all these compounds undergo the typical photochemical *trans*-to-*cis* isomerisation process around the diazenyl unit,<sup>3</sup> the yield and extension of which are out of the scope of this work and have not been quantified.

Alternatively, the spontaneous *cis*-to-*trans* thermal conversion of the solutions of all these compounds, after photochemical excitation, was studied kinetically as a function of solvent, temperature and pressure (Table S1†).<sup>8,11–13</sup> Fig. 1a shows some selected standard changes observed in the UV-Vis spectra after irradiation, and Fig. 1b shows the Eyring and  $\ln k$  *versus*  $P$  plots obtained from the variation of the observed rate constants in toluene and methanol solutions. The full set of derived activation parameters is provided in Table 1.

From the data in Table 1, it is clear that the azo derivatives prepared have different isomerisation mechanisms. While for the new **py-iso** derivative the process is solvent-dependent, with a negative activation volume in the polar solvent studied, for the also new **cyano-iso** derivative the process is completely solvent-independent and slower, with a practically zero activation volume. The data for the already known **iso-iso** diazenyl compound also indicate the solvent independence of the process and a *ca.* zero activation volume. These results clearly indicate that the azo compounds prepared behave in distinct ways, as far as the *cis*-to-*trans* thermal conversion mechanism applies.<sup>12</sup> While for the **py-iso** derivative the collected data clearly point to a mechanism involved in the charge-separated rotational transition state, stabilised by a polar solvent,<sup>52</sup> for the **cyano-iso** and **iso-iso** analogues the process was seen to

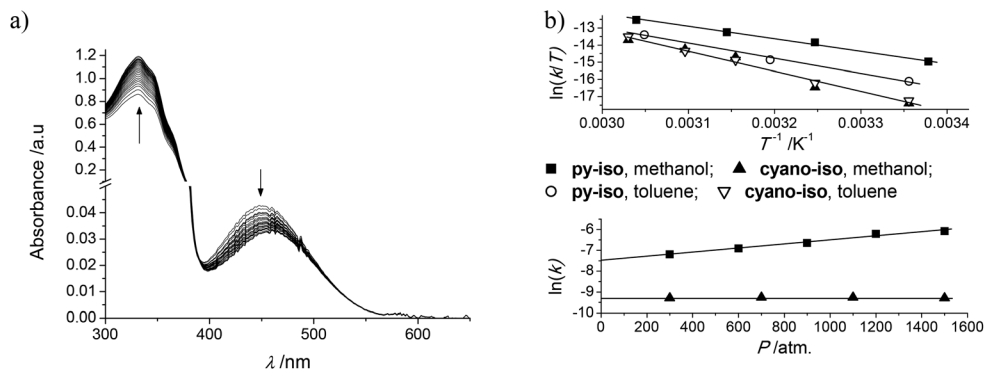


**Fig. 1** (a) UV-Vis spectral changes observed during 4 h of spontaneous thermal *cis*-to-*trans* isomerisation (after photoexcitation of a  $10^{-5}$  M solution of the *cyano-iso* compound) in toluene at 50 °C. (b) Eyring (top) and  $\ln k$  versus  $P$  (bottom) plots for the spontaneous thermal *cis*-to-*trans* processes of the non-symmetric *py-iso* and *cyano-iso* azo ligands studied.

**Table 1** Kinetic (interpolated at 313 K) and activation parameters of the spontaneous thermal *cis*-to-*trans* isomerisation after photoexcitation of the compounds studied in this work (Scheme 2) as a function of the solvent used

Compound	Solvent	${}^{313}k_{cis-to-trans}/s^{-1}$	$\Delta H^\ddagger/kJ\ mol^{-1}$	$\Delta S^\ddagger/J\ K^{-1}\ mol^{-1}$	$\Delta V^\ddagger/cm^3\ mol^{-1}$
<b>py-iso</b>	Toluene	$1.2 \times 10^{-4}$	$72 \pm 4$	$-93 \pm 13$	Not determined
	Methanol	$3.9 \times 10^{-4}$	$61 \pm 3$	$-118 \pm 10$	$-25 \pm 2$ (40 °C)
<b>cyano-iso</b>	Toluene	$5.4 \times 10^{-5}$	$95 \pm 10$	$-26 \pm 30$	Not determined
	Methanol	$7.3 \times 10^{-5}$	$97 \pm 4$	$-17 \pm 13$	<i>ca.</i> 0 (48 °C)
<b>iso-iso</b>	Toluene	$5.7 \times 10^{-5}$	$98 \pm 6$	$-16 \pm 18$	Not determined
	Methanol	$4.4 \times 10^{-5}$	$93 \pm 6$	$-34 \pm 18$	<i>ca.</i> 0 (60 °C)
<b>py-isoFe<sup>II</sup></b>	Methanol	$6.1 \times 10^{-4}$	$78 \pm 8$	$-60 \pm 27$	<i>ca.</i> 0 (25 °C)
	Water	$1.2 \times 10^{-3}$	$76 \pm 4$	$-61 \pm 12$	<i>ca.</i> 0 (35 °C)
<b>cyano-isoFe<sup>II</sup></b>	Methanol	$1.6 \times 10^{-3}$	$89 \pm 3$	$-17 \pm 11$	$19 \pm 2$ (25 °C)
	Water	$4.2 \times 10^{-4}$	$48 \pm 6$	$-160 \pm 20$	Not determined
<b>iso-isoFe<sup>II</sup></b>	Methanol	$9.1 \times 10^{-4}$	$40 \pm 5$	$-178 \pm 17$	Not determined
	Water	$6.9 \times 10^{-4}$	$52 \pm 5$	$-142 \pm 12$	$-6.8 \pm 0.2$ (35 °C)
<b>py-isoFe<sup>III</sup></b>	Water	$1.9 \times 10^{-3}$	$85 \pm 6$	$-28 \pm 19$	$16 \pm 1$ (30 °C)
<b>Fe<sup>II</sup>iso-isoFe<sup>II</sup></b>	Water	$3.3 \times 10^{-4}$	$69 \pm 2$	$-94 \pm 6$	<i>ca.</i> 0 (45 °C)

clearly occur *via* an inversion mechanism, with higher enthalpic requirements and no polar transition state (no ordering/contraction in polar solvents).<sup>9,53</sup>

### Fe<sup>II</sup> azo-pentacyanido complexes

The  $Na_3[(NC)_5Fe^{II}CN(C_6H_4)-N=N-(C_5H_4N)]$  (**py-isoFe<sup>II</sup>**),  $Na_3[(NC)_5Fe^{II}CN(C_6H_4)-N=N-(C_6H_4)CN]$  (**cyano-isoFe<sup>II</sup>**) and  $Na_3[(NC)_5Fe^{II}CN(C_6H_4)-N=N-(C_6H_4)NC]$  (**iso-isoFe<sup>II</sup>**) compounds have been prepared using the reaction of  $[Fe(CN)_5(NH_3)]^{3-}$  with a slight excess of the azo ligand to avoid undesired bridged derivatives (see the Experimental section). The final compounds, which are highly soluble in water, can be easily separated from the excess of ligand by washing with diethyl ether. <sup>13</sup>C NMR clearly shows the attachment of an electron-withdrawing centre to the isocyanide moiety of the azo ligands; for example, on coordination of the azo derivatives, significant signals shift by *ca.* 20 ppm to lower fields (Fig. S2–S4†).<sup>35,37,40</sup> Similarly, in the IR spectra, apart from the signals of the  $\{Fe^{II}(CN)_5^{3-}\}$  unit, the isocyanide stretching

signal at *ca.* 2130  $cm^{-1}$  moves to lower wavenumbers (*ca.* 2070  $cm^{-1}$ ) on Fe<sup>II</sup> coordination.

The UV-Vis spectra of the complexes prepared in methanol and water show interesting features related to the existence of intense CT bands from the metal to the ligand (Fig. 2). These add up to the band on the azo ligand in the 450–500 nm region, producing a rather high intensity at these wavelengths when compared with the free azo derivative. As indicated in the following redox reactivity section, the intensity of that band diminishes, as expected, on Fe<sup>II</sup> to Fe<sup>III</sup> oxidation by peroxodisulfate or electrochemistry. As observed for the free ligands, the <sup>1</sup>H NMR spectra of the irradiated solutions at 365 nm (see Experimental section) show the set of signals that correspond to the *cis* isomer of the diazenyl moiety, apart from the major *trans* isomeric thermally dominant form. The spontaneous back *cis*-to-*trans* thermal conversion of the solutions of these new complexes having a  $\{Fe^{II}(CN)_5^{3-}\}$  fragment attached to the isocyanide group was thus studied, for comparison with that of the free azo ligands, as a function of solvent, temperature and pressure (Table S1†). Fig. S5a† shows

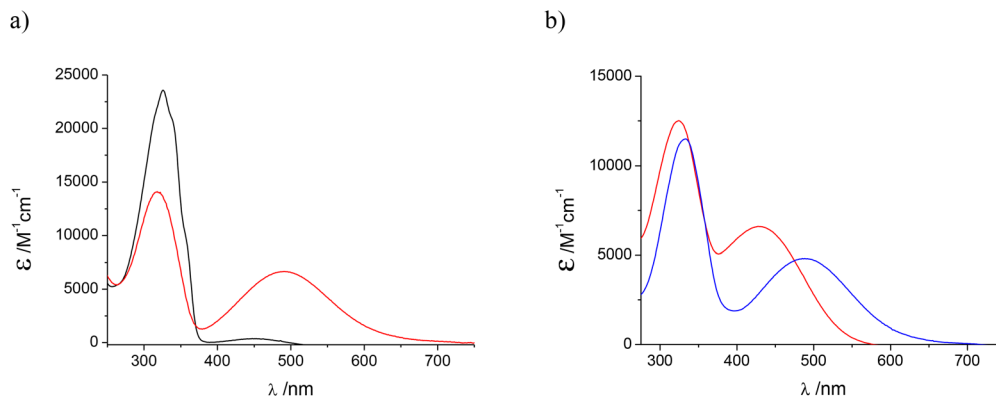


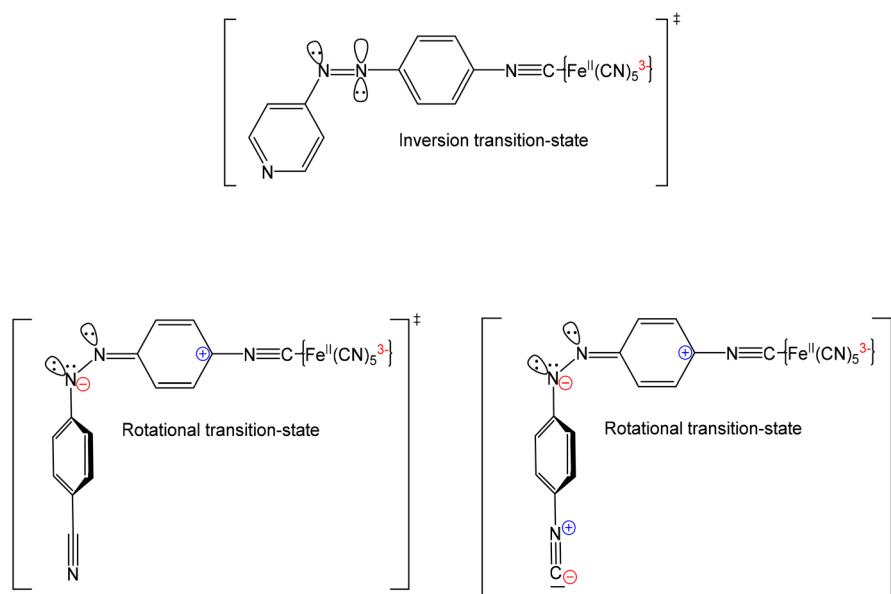
**Fig. 2** (a) UV-Vis spectra of the **py-iso** ligand (black) and its **py-isoFe<sup>II</sup>** derivative (red) in methanol solution. (b) UV-Vis spectra of the **cyano-isoFe<sup>II</sup>** derivative in aqueous (blue) and methanol (red) solutions.

the selected standard changes observed in the UV-Vis spectra after irradiation; it is evident that the UV-Vis spectral changes relate mainly to the MLCT band in the 450–500 nm region, with very little influence on the more intense band around 315 nm. Fig. S5b† shows the corresponding Eyring and  $\ln k$  versus  $P$  plots obtained from the variation of the observed rate constants in aqueous and methanol solutions. The derived activation parameters are provided in Table 1, together with the data for the free azo ligands for comparative purposes.

From the data provided in Table 1, it is clear that important changes must occur in the molecular orbital system of the azo derivatives during the  $\{\text{Fe}^{\text{II}}(\text{CN})_5^{3-}\}$  attachment to their isocyanide group. For all the systems studied, a changeover in the thermal switching mechanism takes place, from charge-separated to inversion (**py-iso**), or from inversion to charge-separated (**cyano-iso** and **iso-iso**), on coordination of the pentacyanidoiron(II) moiety. For the **py-iso** derivative, the arrangement

of the substituents of the starting ligand, which favours a switching mechanism with charge separation, seems to be compensated by the coordination of the  $\{\text{Fe}^{\text{II}}(\text{CN})_5^{3-}\}$  negative moiety (the activation volume changes from  $\Delta V^\ddagger \neq 0$  to  $\Delta V^\ddagger \approx 0$  for all solvents). For the **cyano-iso** and **iso-iso** derivatives, the already symmetric (or quasi-symmetric) arrangement of the substituents in the initial diazenyl compound is disturbed by the coordination of the same  $\{\text{Fe}^{\text{II}}(\text{CN})_5^{3-}\}$  moiety, favouring a change of mechanism to the one showing a charge-separated transition state (the activation volume changing from  $\Delta V^\ddagger \approx 0$  to  $\Delta V^\ddagger \neq 0$ ). By these rearrangements, the possible generation of charged transition states in the *cis-to-trans* back thermal reaction of the azo derivatives (Scheme 3) is hampered or favoured, respectively.

In this respect, the lower contraction observed on going from the free ligands to the  $\{\text{Fe}^{\text{II}}(\text{CN})_5^{3-}\}$ -coordinated species (less negative activation volume, see Table 1) merits some



**Scheme 3** Rotational and inversion transition states.

comment. While charge separation on the free molecules creates compression of the surrounding polar solvent ( $\Delta V^\ddagger = -25 \text{ cm}^3 \text{ mol}^{-1}$  for the **py-iso** ligand), the same process taking place on a  $\{\text{Fe}^{\text{II}}(\text{CN})_5^{3-}\}$ -attached derivative results in a local decrease in positive charge at the isocyanide side of the ligand. This fact implies a lesser degree of compression of the polar solvent molecules (see Scheme 3). As shown in Table 1, this effect is much more pronounced for **cyano-isoFe<sup>II</sup>** ( $\Delta V^\ddagger = +19 \text{ cm}^3 \text{ mol}^{-1}$ ) than for the analogous **iso-isoFe<sup>II</sup>** ( $\Delta V^\ddagger = -6.8 \text{ cm}^3 \text{ mol}^{-1}$ ). The reason is probably related to the fact that for the latter, an extra dipole compensation occurs due to the presence of the dangling isocyanide (Scheme 3).

### Fe<sup>III</sup> azo-pentacyanido complexes

Cyclic voltammetry experiments conducted on the Fe<sup>II</sup> azo-pentacyanido complexes prepared indicate that the three new compounds can be reversibly oxidised to their Fe<sup>III</sup> derivatives (Fig. 3a). Furthermore, the spectroelectrochemical forward and back titrations of the complex  $[(\text{NC})_5\text{Fe}^{\text{II}}\text{CN}(\text{C}_6\text{H}_4)\text{-N}=\text{N}(\text{C}_5\text{H}_4\text{N})]^{3-}$  were also conducted (Fig. 3b) to measure the neat and fully reversible nature of the process.

In view of this well-behaved redox process, and our interest in the use of these Fe<sup>II</sup> azo-pentacyanido derivatives as building blocks for mixed-valence polynuclear species,<sup>35,40</sup> the chemical oxidation of  $[(\text{NC})_5\text{Fe}^{\text{II}}\text{CN}(\text{C}_6\text{H}_4)\text{-N}=\text{N}(\text{C}_5\text{H}_4\text{N})]^{3-}$  with  $\text{S}_2\text{O}_8^{2-}$  was also studied as a model of the other two azo ligand coordination derivatives prepared in this work.<sup>54-56</sup> The process thus monitored results in neat UV-Vis spectral changes that parallel those observed in the spectroelectrochemical Fe<sup>II</sup>-to-Fe<sup>III</sup> titration (Fig. S6†). From these changes, and under pseudo-first order conditions (see the Experimental section), the set of  $k_{\text{obs}}$  values provided in Table S2† were derived at different  $\text{S}_2\text{O}_8^{2-}$  concentrations, temperatures and pressures. Fig. 4a shows a summary of the changes observed for the values of  $k_{\text{obs}}$  on  $[\text{S}_2\text{O}_8^{2-}]$ ; Fig. 4b shows the temperature and pressure dependence of the slopes of these plots.<sup>57,58</sup> The thermal activation data derived ( $\Delta H^\ddagger = 64 \pm 5 \text{ kJ mol}^{-1}$ ;  $\Delta S^\ddagger = -58 \pm 16 \text{ J K}^{-1} \text{ mol}^{-1}$ ) lie within the expected values for these types of processes, where an {outer-sphere precursor complex}-non-limited rate law applies (*i.e.*  $k_{\text{obs}} = k_{\text{et}} \times K_{\text{OS}}[\text{S}_2\text{O}_8^{2-}]$ ).<sup>40,57,59,60</sup> On the other hand, the value of the activation volume for the second-order rate constant (*i.e.*  $k_{\text{et}} \times K_{\text{OS}}$ )

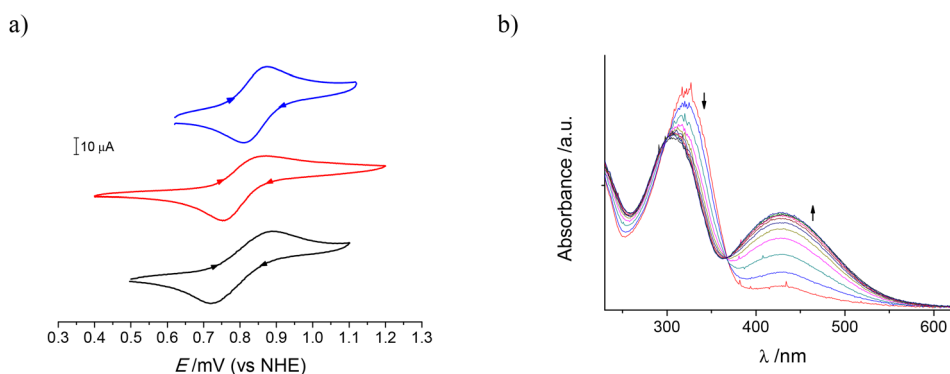


**Fig. 3** (a) CV of aqueous solutions of  $\text{Na}_3[(\text{NC})_5\text{Fe}^{\text{II}}\text{CN}(\text{C}_6\text{H}_4)\text{-N}=\text{N}(\text{C}_5\text{H}_4\text{N})]$  (black),  $\text{Na}_3[(\text{NC})_5\text{Fe}^{\text{II}}\text{CN}(\text{C}_6\text{H}_4)\text{-N}=\text{N}(\text{C}_6\text{H}_4\text{CN})]$  (red), and  $\text{Na}_3[(\text{NC})_5\text{Fe}^{\text{II}}\text{CN}(\text{C}_6\text{H}_4)\text{-N}=\text{N}(\text{C}_6\text{H}_4\text{NC})]$  (blue) at  $200 \text{ mV s}^{-1}$  (conditions stated in the Experimental section). (b) Spectroelectrochemical back titration at  $0.500 \text{ V}$  for the  $[(\text{NC})_5\text{Fe}^{\text{III}}\text{CN}(\text{C}_6\text{H}_4)\text{-N}=\text{N}(\text{C}_5\text{H}_4\text{N})]^{2-}$  compound obtained after electrochemical oxidation of a  $\text{Na}_3[(\text{NC})_5\text{Fe}^{\text{II}}\text{CN}(\text{C}_6\text{H}_4)\text{-N}=\text{N}(\text{C}_5\text{H}_4\text{N})]$  solution.

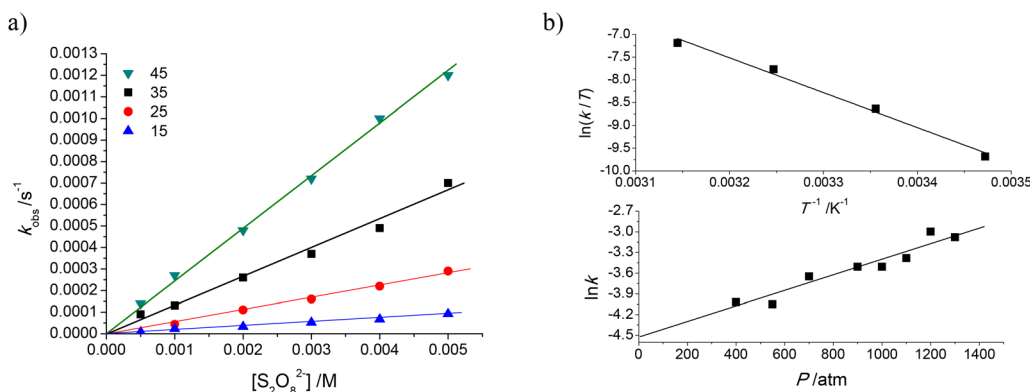


**Fig. 4** (a) Dependence of the pseudo-first order rate constants observed for the oxidation of  $[(\text{NC})_5\text{Fe}^{\text{II}}\text{CN}(\text{C}_6\text{H}_4)\text{-N}=\text{N}(\text{C}_5\text{H}_4\text{N})]^{3-}$  with  $\text{S}_2\text{O}_8^{2-}$  at different temperatures and  $l = 0.20 \text{ M}$  ( $\text{NaClO}_4$ ). (b) Eyring (top) and  $\ln k$  versus  $P$  (bottom) plots for the same reaction.

is clearly negative ( $\Delta V^\ddagger = -29 \pm 3 \text{ cm}^3 \text{ mol}^{-1}$ ), which is opposite to all the values determined so far for these types of {outer-sphere precursor complex}-non-limited reactions, where  $\Delta V^\ddagger = \Delta V_{(\text{OS})}^0 + \Delta V_{(\text{et})}^\ddagger$ .<sup>40,57</sup> Only for reactions occurring under the {outer-sphere precursor complex}-limited rate law (*i.e.*  $k_{\text{obs}} = k_{\text{et}} \times K_{\text{OS}}[\text{S}_2\text{O}_8^{2-}]/(1 + K_{\text{OS}}[\text{S}_2\text{O}_8^{2-}])$ ),<sup>59,60</sup> the values have been found to be negative when derived from the isolated first-order rate constant (*i.e.*  $\Delta V_{(\text{et})}^\ddagger$ ,  $k_{\text{et}}$ ).<sup>37</sup> In our case, this rate law is not observed and the negative value obtained has to be associated with a practically zero value of  $\Delta V^0$  for  $K_{\text{OS}}$  (making  $\Delta V^\ddagger \approx \Delta V_{(\text{et})}^\ddagger$ ), thus corroborating the important role of the dangling azo ligand in the process.

In view of the neat process observed, the important redox reactivity of the mixed valence compounds containing  $\{\text{Fe}(\text{CN})_6\}$  units, and the differences observed in the *cis-to-trans* thermal isomerisation mechanism on metal coordination to the isocyanide substituents, the *in situ* preparation of the  $[(\text{NC})_5\text{Fe}^{\text{III}}\text{CN}(\text{C}_6\text{H}_4)\text{-N}=\text{N}(\text{C}_5\text{H}_4\text{N})]^{2-}$  oxidised derivative was pursued. Effectively, following the above results (Fig. 4a and Table S2<sup>†</sup>), a  $1 \times 10^{-5} \text{ M}$  aqueous solution of  $[(\text{NC})_5\text{Fe}^{\text{II}}\text{CN}(\text{C}_6\text{H}_4)\text{-N}=\text{N}(\text{C}_5\text{H}_4\text{N})]^{3-}$  was maintained in a  $5 \times 10^{-4} \text{ M}$  solution of  $\text{Na}_2\text{S}_2\text{O}_8$  for 24 h at 35 °C (checked for completion by monitoring the UV-Vis spectral changes, see Fig. S6<sup>†</sup>). The final solution obtained was irradiated at 365 nm, and the back *cis-to-trans* thermal switching process was kinetically monitored at different temperatures and pressures (Table S1<sup>†</sup>). The values thus obtained are indicative of the extremely important role played by the moieties attached to the isocyanide group of the azo derivative (Fig. 5). A summary of these values is provided in Table 1 for comparison with the remaining data available.

From the data, it is clear that a shift in the isomerisation mechanism has occurred on going from the  $\{\text{Fe}^{\text{II}}(\text{CN})_5\}^{3-}$  to the  $\{\text{Fe}^{\text{III}}(\text{CN})_5\}^{2-}$  coordination to the  $\text{CN}(\text{C}_6\text{H}_4)\text{-N}=\text{N}(\text{C}_5\text{H}_4\text{N})$  azo ligand. The process clearly reverts to a charge-separated isomerisation process, as indicated by  $\Delta V^\ddagger \neq 0$  (Fig. 5b). The value of the activation volume again indicates an expansion, as for the  $\text{Fe}^{\text{II}}$ -coordinated derivative, and the same reasons indicated in the previous section apply. The generated positive charge is absorbed by the negative  $\{\text{Fe}^{\text{III}}(\text{CN})_5\}^{2-}$  moiety, thus

producing an expansion of the polar solvent molecules and a positive activation volume (see Table 1).

### $(\text{Fe}^{\text{II}})_2$ azo-pentacyanido complexes

In view of the robustness of the water soluble  $\text{Fe}^{\text{II}}$  azo-pentacyanido complexes obtained, plus that the compounds derived from the **py-iso** and **iso-iso** azo ligands are capable of facile coordination to two  $\{\text{Fe}^{\text{II}}(\text{CN})_5\}^{3-}$  moieties, the preparation of bimetallic compounds  $\text{Fe}^{\text{II}}\text{py-isoFe}^{\text{II}}$  and  $\text{Fe}^{\text{II}}\text{iso-isoFe}^{\text{II}}$  was pursued. As indicated in the Experimental section, the desired compounds can be prepared in a straightforward manner using either a 2 : 1 mixture ratio of the iron : azo compounds, or a 1 : 1 mixture of the **py-isoFe}^{\text{II}}** or **iso-isoFe}^{\text{II}}** species and the  $[\text{Fe}^{\text{II}}(\text{CN})_5(\text{NH}_3)]^{3-}$  precursor. For the  $\text{Fe}^{\text{II}}\text{iso-isoFe}^{\text{II}}$  complex, the  $^1\text{H}$  and  $^{13}\text{C}$  NMR spectra (Fig. S7<sup>†</sup>) clearly indicate the full symmetric nature of the species prepared, while electrochemical experiments show the presence of two quasi-reversible oxidation processes at 840 and 1080 mV (Fig. 6a). The UV-Vis spectrum is also indicative of the coordination of two  $\text{Fe}^{\text{II}}$  centres to the azo ligand, as the band MLCT at *ca.* 435 nm has a higher intensity than the one for the **iso-isoFe}^{\text{II}}** derivative (Fig. 6b). For the  $\text{Fe}^{\text{II}}\text{py-isoFe}^{\text{II}}$  complex, the  $^1\text{H}$  NMR obtained immediately on dissolution in  $\text{D}_2\text{O}$ , produces the expected signals (Fig. S8a<sup>†</sup>) and the electrochemical experiments clearly indicate the occurrence of two distinct and differentiated iron oxidation processes at 480 and 840 mV for the pyridine- and isocyanide-attached iron centres, respectively (Fig. S8b<sup>†</sup>). Nevertheless, on standing for *ca.* two hours the  $^1\text{H}$  NMR also shows signals of the **py-isoFe}^{\text{II}}** complex, thus indicating that, although the desired  $\text{Fe}^{\text{II}}\text{py-isoFe}^{\text{II}}$  species is kinetically formed, it evolves to the thermodynamically more stable **py-isoFe}^{\text{II}}** and  $[\text{Fe}^{\text{II}}(\text{CN})_5(\text{H}_2\text{O})]^{3-}$  on standing. Effectively, the  $^{13}\text{C}$  NMR spectrum of a  $\text{D}_2\text{O}$  solution of the aged sample shows the signals associated with the **py-isoFe}^{\text{II}}** and  $[\text{Fe}^{\text{II}}(\text{CN})_5(\text{H}_2\text{O})]^{3-}$  components (Fig. S8c<sup>†</sup>). Given the fact that the UV-vis spectroscopic study of the actual  $\text{Fe}^{\text{II}}\text{py-isoFe}^{\text{II}} \rightarrow \text{py-isoFe}^{\text{II}} + [\text{Fe}^{\text{II}}(\text{CN})_5(\text{H}_2\text{O})]^{3-}$  reaction (Fig. S9<sup>†</sup>) shows that the ejection of the  $\{\text{Fe}^{\text{II}}(\text{CN})_5\}^{3-}$  moiety from the complex takes place at the same, or even shorter, time scale than that of the expected *cis-to-trans* thermal reactions studied in this work, we

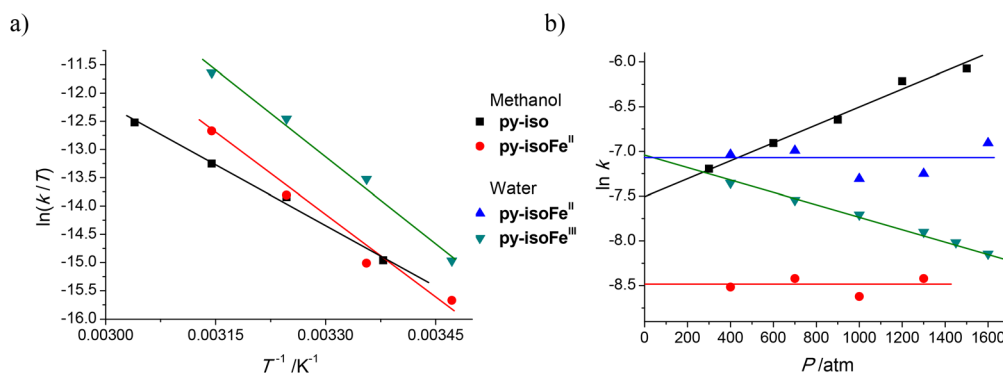
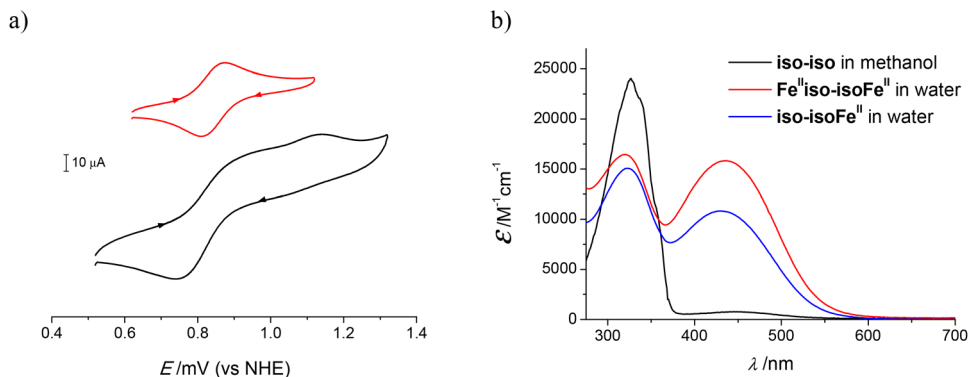


Fig. 5 Variation of the thermal (a) and pressure (b) activation parameters for the *cis-to-trans* isomerisation process occurring on the  $\text{CN}(\text{C}_6\text{H}_4)\text{-N}=\text{N}(\text{C}_5\text{H}_4\text{N})$  azo ligand depending on its coordination (free,  $\text{Fe}^{\text{II}}$  or  $\text{Fe}^{\text{III}}$ ).



**Fig. 6** (a) CV of aqueous solutions of  $\text{Na}_6[(\text{NC})_5\text{Fe}^{\text{II}}\text{CN}(\text{C}_6\text{H}_4)\text{-N=N-(C}_6\text{H}_4\text{)NCFe}^{\text{II}}(\text{CN})_5]$  and  $\text{Na}_3[(\text{NC})_5\text{Fe}^{\text{II}}\text{CN}(\text{C}_6\text{H}_4)\text{-N=N-(C}_6\text{H}_4\text{)NC}]$  at  $200 \text{ mV s}^{-1}$  (conditions stated in the Experimental section). (b) UV-Vis spectra of the same compounds.

did not further consider the photoswitching of this new compound.

In contrast, as observed in the NMR spectra, the photochemical excitation of the dinuclear  $\text{Fe}^{\text{II}}\text{iso-isoFe}^{\text{II}}$  compound at 365 nm is, again, easily achieved and the *cis* isomeric form obtained shows notable differences in the UV-Vis spectrum that allow the monitoring of the back thermal *cis*-to-*trans* reaction. Similarly to the  $\text{py-isoFe}^{\text{II}}$ ,  $\text{cyano-isoFe}^{\text{II}}$ ,  $\text{iso-isoFe}^{\text{II}}$ , and  $\text{py-isoFe}^{\text{III}}$  derivatives (see for example Fig. S5a†), these differences are mainly related to the increase in the intensity of the MLCT band at 435 nm, as seen in Fig. S10,† without the typical changes observed for the free azo ligands (Fig. 1a). The changes of the first-order rate constants for this thermal switching process, with respect to temperature and pressure, produce the set of activation parameters that are also provided in Table 1 for comparison. From the data, it is clear that the thermal *cis*-to-*trans* isomerisation process occurring for this doubly substituted highly charged {6+} complex has the same mechanistic characteristics as those of the original symmetric  $\text{iso-iso}$  azo ligand, *i.e.*, an inversion transition state ( $\Delta V^\ddagger = 0$ ). Even so, the differences in the thermal activation parameters are rather important and can be attributed to the dramatic changes in the charge of the bis- $\{\text{Fe}^{\text{II}}(\text{CN})_5^{3-}\}$  azo species, which changes from {0} to {6+}.

## Conclusions

The design and preparation of new azo derivatives with good coordinating groups at the *para* positions of their phenyl rings is feasible, and compounds having pyridine, cyano and isocyano groups have been synthesized and fully characterised. Their use as linkers in the formation of water-soluble metallic compounds has been achieved by coordination to  $\{\text{Fe}^{\text{II}}(\text{CN})_5^{3-}\}$  units, in one or two of the anchoring groups of the organic derivatives. The coordination occurs in such a manner that the standard *trans/cis* photoisomerisation is still possible, as the diazenyl group is not involved in the coordination of the metals, thus providing a switching capability of the assemblies. The back *cis*-to-*trans* thermal isomerisation process of

these metal complexes has been studied thoroughly as a function of the donor groups, solvent, temperature and pressure, in order to gain insight into the rotational or inversional mechanisms involved in this reaction. This mechanism has been compared with that occurring on the free azo derivatives. Surprisingly, a relevant tuning of the process is observed on coordination of the  $\{\text{Fe}^{\text{II}}(\text{CN})_5^{3-}\}$  moieties to a single or both phenyl groups of the diazenyl-containing molecules, or on oxidation of the iron centre to obtain  $\{\text{Fe}^{\text{III}}(\text{CN})_5^{3-}\}$ -attached compounds. These differences are especially relevant as some of these processes could be hindered on formation of polymetallic structures, depending on the thermal *cis*-to-*trans* isomerisation mechanism actuated, thus producing non-photoswitchable entities that have been generated from photoactive linkers.

## Experimental

### Physical methods

The  $^1\text{H}$  and  $^{13}\text{C}\{^1\text{H}\}$  NMR spectra were recorded on a Bruker-400 or 500 spectrophotometer at 25 °C; the infrared spectra were recorded on an FT-IR 5700 Nicolet spectrophotometer; and the ESI mass spectra were recorded on an LC/MSD TOF Agilent Technologies 61969A instrument in methanol or acetonitrile solutions. Photochemical *trans*-to-*cis* excitation of the azo derivatives was carried out using an ASAHI MAX-303 light source equipped with the desired filters.

Electrochemical CV experiments were carried out at 25 °C and 100 or 200  $\text{mV s}^{-1}$ , using a BioLogic SP-150 instrument. A glassy carbon working electrode, an Ag/AgCl (saturated KCl) reference electrode and a platinum wire counter electrode were used in  $1 \times 10^{-3} \text{ M}$  solutions of the sample, and 0.1 M  $\text{NaClO}_4$  was used as the supporting electrolyte for aqueous solutions. For acetonitrile solutions, a glassy carbon working electrode, an Ag/AgNO<sub>3</sub> (acetonitrile) reference electrode, and a platinum wire counter electrode were used in  $1 \times 10^{-3} \text{ M}$  solutions of the sample. 0.1 M  $\text{Bu}_4\text{NClO}_4$  was used as the supporting electrolyte, and the potentials were referenced externally against the ferrocene/ferrocenium pair (+640 mV).<sup>61</sup> All potentials are

given against the NHE, once corrected for the reference electrode used.

Spectroelectrochemical titrations were performed in  $7 \times 10^{-5}$  M solutions of the iron complexes in  $\text{H}_2\text{O}$  ( $\text{pH} = 7.0$ ,  $I = 0.1$  M  $\text{NaClO}_4$ ) at 0.92 V vs. the NHE, according to the CV indicated in Fig. 2a, using a platinum flag working electrolyte, an Ag/AgCl/sat. KCl reference electrode and a platinum counter electrode. The UV-Vis spectra were recorded using a Helma 661.202-UV All Quartz Immersion Probe set in the titration vessel and connected to a Cary50 instrument with optical fibres; the full spectra were fitted using Reactlab.<sup>62</sup> Back titrations were conducted at 0.500 V using the same setup.

The kinetic profiles for the reactions under atmospheric pressure were followed by UV-Vis spectroscopy in the 900–300 nm range using a Cary50 or an Agilent HP8453A instrument equipped with thermostated multicell transports at 0.2 M ionic strength ( $\text{NaClO}_4$ ). For runs at elevated pressures, the previously described high-pressure set-up<sup>12,63</sup> was used, connected to a J&M TIDAS S300 instrument. The full operative system and software<sup>62,64</sup> used for the determination of the first order rate constants involved have already been described.<sup>8,13,35</sup> All post-run fittings were carried out using the standard available commercial programs. In all instances, the rate constants were the average of two or three replicates with an error between 10 and 15%.

XRD measurements were conducted on an orange needle-like specimen (*ca.*  $0.044 \times 0.079 \times 0.412$  mm); the X-ray intensity data were measured on a D8 Venture system equipped with a multilayer monochromator and a Mo microfocus ( $\lambda = 0.71073$  Å). The frames were integrated with the Bruker SAINT software package using a narrow-frame algorithm.<sup>65</sup> The integration of the data using a monoclinic unit cell yielded a total of 11 648 reflections to a maximum  $\theta$  angle of  $30.59^\circ$  ( $0.70$  Å resolution), of which 3143 were independent (average redundancy: 3.706, completeness = 100.0%,  $R_{\text{int}} = 3.10\%$ ,  $R_{\text{sig}} = 2.85\%$ ) and 2705 (86.06%) were greater than  $2\sigma(F^2)$ . The final cell constants  $a = 4.6702(3)$  Å,  $b = 10.4251(7)$  Å,  $c = 11.8640(8)$  Å,  $\beta = 98.307(3)^\circ$ , and volume =  $571.57(7)$  Å<sup>3</sup> are based on the refinement of the XYZ centroids of reflections above  $20 \sigma(I)$ . Data were corrected for absorption effects using a multi-scan method (SADABS).<sup>66</sup> The calculated minimum and maximum transmission coefficients (based on the crystal size) were 0.6846 and 0.7461, respectively. The structure was resolved and refined using the Bruker SHELXTL software package,<sup>67</sup> using the space group *Pc*, with  $Z = 2$  for the formula unit,  $\text{C}_{14}\text{H}_8\text{N}_4$ . The structure was resolved and refined using the Bruker SHELXTL software package, using the space group *P1c1*, with  $Z = 2$  for the formula unit,  $\text{C}_{14}\text{H}_8\text{N}_4$ . The final anisotropic full-matrix least-squares refinement on  $F^2$  with 164 variables converged at  $R_1 = 4.16\%$  for the observed data and  $wR_2 = 11.35\%$  for all data. The goodness-of-fit was 1.027. The largest peak in the final difference electron density synthesis was  $0.336 \text{ e}^- \text{ \AA}^{-3}$  and the largest hole was  $-0.250 \text{ e}^- \text{ \AA}^{-3}$  with an RMS deviation of  $0.047 \text{ e}^- \text{ \AA}^{-3}$ . On the basis of the final model, the calculated density was  $1.349 \text{ g cm}^{-3}$  and  $F(000)$ , 240  $e^-$ . CCDC code: 2216961.†

## Materials and compounds

All chemicals and solvents used in the preparations were of analytical grade, commercially available and used as received. All the azo ligands have been prepared by optimisation of the literature methods<sup>47,68</sup> and the details are shown in the ESI.†

## Synthesis of iron compounds

$\text{Na}_3[(\text{NC})_5\text{Fe}^{\text{II}}\text{CN}(\text{C}_6\text{H}_4)\text{-N=N-(C}_5\text{H}_4\text{N)}]$ , **py-isoFe<sup>II</sup>**. 300 mg (1.4 mmol) of  $\text{CN}(\text{C}_6\text{H}_4)\text{-N=N-(C}_5\text{H}_4\text{N)}$  was dissolved in a purged 60 mL MeOH and 6 mL  $\text{H}_2\text{O}$  mixture in a Schlenk tube. After complete dissolution, 325 mg (1.0 mmol) of solid  $\text{Na}_3[\text{Fe}^{\text{II}}(\text{CN})_5(\text{NH}_3)] \cdot 3\text{H}_2\text{O}$ <sup>69,70</sup> was added and the mixture was left stirring overnight, protected from light under a nitrogen atmosphere. The resulting solution was dried to obtain a deep red residue, which was thoroughly washed several times with diethyl ether, yielding the final  $\text{Na}_3[(\text{NC})_5\text{Fe}^{\text{II}}\text{CN}(\text{C}_6\text{H}_4)\text{-N=N-(C}_5\text{H}_4\text{N)}]$  compound (300 mg, 65% yield). <sup>1</sup>H NMR ( $\text{D}_2\text{O}$ , 400 MHz):  $\delta$  (*trans*) 8.77 (d,  $J_{\text{HH}} = 6.4$  Hz, 2H,  $\text{H}_{\alpha\text{-py}}$ ), 8.04 (d,  $J_{\text{HH}} = 8.7$  Hz, 2H,  $\text{H}_{\text{meta}}\text{PhNC}$ ), 7.82 (d,  $J_{\text{HH}} = 6.4$  Hz, 2H,  $\text{H}_{\beta\text{-py}}$ ), 7.72 (d,  $J_{\text{HH}} = 8.7$  Hz, 2H,  $\text{H}_{\text{ortho}}\text{PhNC}$ ); (*cis* after irradiation) 9.18 (d,  $J_{\text{HH}} = 6.8$  Hz, 2H,  $\text{H}_{\alpha\text{-py}}$ ), 7.65 (d,  $J_{\text{HH}} = 6.7$  Hz, 2H), 7.54 (d,  $J_{\text{HH}} = 6.8$  Hz, 2H). <sup>1</sup>H NMR ( $\text{CD}_3\text{OD}$ , 400 MHz):  $\delta$  (*trans*) 8.76 (d,  $J_{\text{HH}} = 6.2$  Hz, 2H,  $\text{H}_{\alpha\text{-py}}$ ), 8.02 (d,  $J_{\text{HH}} = 9.0$  Hz, 2H,  $\text{H}_{\text{meta}}\text{PhNC}$ ), 7.85 (d,  $J_{\text{HH}} = 6.2$  Hz, 2H,  $\text{H}_{\beta\text{-py}}$ ), 7.62 (d,  $J_{\text{HH}} = 9.0$  Hz, 2H,  $\text{H}_{\text{ortho}}\text{PhNC}$ ). <sup>13</sup>C NMR ( $\text{D}_2\text{O}$ , 100.6 MHz):  $\delta$  (*trans*) 182.9 ( $\text{FeCN}_{\text{bridge}}$ ), 168.8 ( $\text{FeCN}_{\text{terminal}}$ ), 157.8 ( $\text{C}_{\text{q-N=N}}$ ), 150.5 ( $\text{C}_{\alpha\text{-py}}$ ), 150.4 ( $\text{C}_{\text{q-N=N}}$ ), 132.8 ( $\text{C}_{\text{q-NC}}$ ), 127.2 ( $\text{C}_{\text{ortho}}\text{PhNC}$ ), 124.4 ( $\text{C}_{\text{meta}}\text{PhNC}$ ), 116.5 ( $\text{C}_{\beta\text{-py}}$ ). IR ( $\nu_{\text{CN}}$ ): 2135, 2070  $\text{cm}^{-1}$ . MS (ESI+)  $m/z$ :  $\{[(\text{NC})_5\text{Fe}^{\text{II}}\text{CN}(\text{C}_6\text{H}_4)\text{-N=N-(C}_5\text{H}_4\text{N)}]^{3-} + 4\text{H}^+\}^+$ , 398.05 (calc. 398.06);  $\{[(\text{NC})_5\text{Fe}^{\text{II}}\text{CN}(\text{C}_6\text{H}_4)\text{-N=N-(C}_5\text{H}_4\text{N)}]^{3-} + \text{Na}^+ + 3\text{H}^+\}^+$ , 420.04 (calc. 420.04);  $\{[(\text{NC})_5\text{Fe}^{\text{II}}\text{CN}(\text{C}_6\text{H}_4)\text{-N=N-(C}_5\text{H}_4\text{N)}]^{3-} + 2\text{Na}^+ + 2\text{H}^+\}^+$ , 442.02 (calc. 442.02). UV-vis [ $\lambda_{\text{max}}$ , nm ( $\epsilon$ ,  $\text{M}^{-1} \text{ cm}^{-1}$ )] (water) 305 (11 500), 430 (6000); (methanol) 318 (14 300), 490 (6600). CV (aqueous solution,  $E^\circ$  vs. NHE): 835 mV plus the irreversible reduction wave at  $-570$  mV.

$\text{Na}_3[(\text{NC})_5\text{Fe}^{\text{II}}\text{CN}(\text{C}_6\text{H}_4)\text{-N=N-(C}_6\text{H}_4\text{CN)}]$ , **cyano-isoFe<sup>II</sup>**. This compound was prepared following the same procedure indicated for the  $\text{Na}_3[(\text{NC})_5\text{Fe}^{\text{II}}\text{CN}(\text{C}_6\text{H}_4)\text{-N=N-(C}_5\text{H}_4\text{N)}]$  analogue but doubling the MeOH volume due to solubility issues. From 300 mg (1.3 mmol) of  $\text{CN}(\text{C}_6\text{H}_4)\text{-N=N-(C}_5\text{H}_4\text{CN)}$  and 325 mg (1.0 mmol) of  $\text{Na}_3[\text{Fe}^{\text{II}}(\text{CN})_5(\text{NH}_3)] \cdot 3\text{H}_2\text{O}$ , 320 mg of the desired compound was obtained (66% yield). <sup>1</sup>H NMR ( $\text{D}_2\text{O}$ , 400 MHz):  $\delta$  (*trans*) 8.03–7.99 (m, 6H,  $\text{H}_{\text{meta}}\text{PhCN} + \text{H}_{\text{meta}}\text{PhNC} + \text{H}_{\text{ortho}}\text{PhCN}$ ), 7.70 (d,  $J_{\text{HH}} = 8.9$  Hz, 2H,  $\text{H}_{\text{ortho}}\text{PhNC}$ ); (*cis*) 7.75 (d,  $J_{\text{HH}} = 8.6$  Hz, 2H,  $\text{H}_{\text{meta}}\text{PhCN}$ ), 7.43 (d,  $J_{\text{HH}} = 8.8$  Hz, 2H,  $\text{H}_{\text{meta}}\text{PhNC}$ ), 7.11 (d,  $J_{\text{HH}} = 8.7$  Hz, 2H,  $\text{H}_{\text{ortho}}\text{PhCN}$ ), 7.03 (d,  $J_{\text{HH}} = 8.8$  Hz, 2H,  $\text{H}_{\text{ortho}}\text{PhNC}$ ). <sup>1</sup>H NMR ( $\text{CD}_3\text{OD}$ , 400 MHz):  $\delta$  (*trans*) 8.09–8.05 (m, 4H,  $\text{H}_{\text{meta}}\text{PhCN} + \text{H}_{\text{meta}}\text{PhNC}$ ), 7.96 (d,  $J_{\text{HH}} = 8.8$  Hz, 2H,  $\text{H}_{\text{ortho}}\text{PhCN}$ ), 7.69 (d,  $J_{\text{HH}} = 8.7$  Hz, 2H,  $\text{H}_{\text{ortho}}\text{PhNC}$ ); (*cis*) 7.70 (d,  $J_{\text{HH}} = 8.7$  Hz, 2H,  $\text{H}_{\text{meta}}\text{PhCN}$ ), 7.34 (d,  $J_{\text{HH}} = 8.7$  Hz, 2H,  $\text{H}_{\text{meta}}\text{PhNC}$ ), 7.02 (d,  $J_{\text{HH}} = 8.5$  Hz, 2H,  $\text{H}_{\text{ortho}}\text{PhCN}$ ), 6.90 (d,  $J_{\text{HH}} = 8.7$  Hz, 2H,  $\text{H}_{\text{ortho}}\text{PhNC}$ ). <sup>13</sup>C NMR ( $\text{CD}_3\text{OD}$ , 125.7 MHz):  $\delta$  (*trans*) 192.9 ( $\text{FeCN}_{\text{bridge}}$ ), 167.8 ( $\text{FeCN}_{\text{terminal}}$ ), 167.6 ( $\text{FeCN}_{\text{terminal}}$ ), 156.0 ( $\text{C}_{\text{q-N=N}}$ ), 151.5 ( $\text{C}_{\text{q-N=N}}$ ), 135.4 ( $\text{C}_{\text{q-NC}}$ ), 134.6 ( $\text{C}_{\text{ortho}}\text{PhCN}$ ), 127.9

(*C*<sub>ortho</sub>PhNC), 125.5 (*C*<sub>meta</sub>PhNC), 124.5 (*C*<sub>meta</sub>PhNC), 119.3 (CN), 115.2 (C<sub>q</sub>-CN). IR ( $\nu_{\text{CN}}$ ): 2244, 2133, 2071 cm<sup>-1</sup>. MS (ESI<sup>-</sup>) *m/z*: {[(NC)<sub>5</sub>Fe<sup>II</sup>CN(C<sub>6</sub>H<sub>4</sub>)-N=N-(C<sub>6</sub>H<sub>4</sub>)CN]<sup>3-</sup> + 2H<sup>+</sup>}<sup>-</sup>, 420.04 (calc. 420.04); {[(NC)<sub>5</sub>Fe<sup>II</sup>CN(C<sub>6</sub>H<sub>4</sub>)-N=N-(C<sub>6</sub>H<sub>4</sub>)CN]<sup>3-</sup> + Na<sup>+</sup> + H<sup>+</sup>}<sup>-</sup>, 442.02 (calc. 442.02). UV-vis [ $\lambda_{\text{max}}$ , nm ( $\epsilon$ , M<sup>-1</sup> cm<sup>-1</sup>)] (water) 325 (12 500), 428 (6600); (methanol) 330 (11 500), 486 (4800). CV (aqueous solution, E° vs. NHE): 815 mV plus the irreversible reduction wave at -680 mV.

**Na<sub>3</sub>[(NC)<sub>5</sub>Fe<sup>II</sup>CN(C<sub>6</sub>H<sub>4</sub>)-N=N-(C<sub>6</sub>H<sub>4</sub>)NC], iso-isoFe<sup>II</sup>.** 115 mg (0.5 mmol) of finely powdered CN(C<sub>6</sub>H<sub>4</sub>)-N=N-(C<sub>6</sub>H<sub>4</sub>)NC was stirred in 80 mL of purged MeOH in a Schlenk flask. Then, 35 mg (0.1 mmol) of solid Na<sub>3</sub>[Fe<sup>II</sup>(CN)<sub>5</sub>(NH<sub>3</sub>)<sub>3</sub>].3H<sub>2</sub>O was added in little portions and the mixture was left stirring for 30 min, protected from light under a nitrogen atmosphere. The resulting solution was dried to obtain a red residue, which was thoroughly washed several times with diethyl ether, yielding the final Na<sub>3</sub>[(NC)<sub>5</sub>Fe<sup>II</sup>CN(C<sub>6</sub>H<sub>4</sub>)-N=N-(C<sub>6</sub>H<sub>4</sub>)NC] compound (20 mg, 41% yield). <sup>1</sup>H NMR (D<sub>2</sub>O, 500 MHz):  $\delta$  (*trans*) 7.98 (m, 4H, H<sub>meta</sub>PhNC), 7.71 (m, 4H, H<sub>ortho</sub>PhNC); (*cis*) 7.47 (d, *J*<sub>HH</sub> = 8.7 Hz, 2H, H<sub>meta</sub>PhNC), 7.43 (d, *J*<sub>HH</sub> = 8.8 Hz, 2H, H<sub>meta</sub>PhNC), 7.05 (d, *J*<sub>HH</sub> = 8.8 Hz, 2H, H<sub>ortho</sub>PhNC), 7.02 (d, *J*<sub>HH</sub> = 8.7 Hz, 2H, H<sub>ortho</sub>PhNC). <sup>1</sup>H NMR (CD<sub>3</sub>OD, 400 MHz):  $\delta$  (*trans*) 8.02 (d, *J*<sub>HH</sub> = 8.7 Hz, 4H, H<sub>meta</sub>PhNC), 7.96 (d, *J*<sub>HH</sub> = 8.8 Hz, 2H, H<sub>meta</sub>PhNC), 7.65 (d, *J*<sub>HH</sub> = 8.7 Hz, 2H, H<sub>ortho</sub>PhNC), 7.60 (d, *J*<sub>HH</sub> = 8.7 Hz, 2H, H<sub>ortho</sub>PhNC); (*cis*) 7.43 (d, *J*<sub>HH</sub> = 8.5 Hz, 2H, H<sub>meta</sub>PhNC), 7.35 (d, *J*<sub>HH</sub> = 8.7 Hz, 2H, H<sub>meta</sub>PhNC), 6.96 (d, *J*<sub>HH</sub> = 8.6 Hz, 2H, H<sub>ortho</sub>PhNC), 6.89 (d, *J*<sub>HH</sub> = 8.7 Hz, 2H, H<sub>ortho</sub>PhNC). <sup>13</sup>C NMR (D<sub>2</sub>O, 100.6 MHz):  $\delta$  (*trans*) 182.3 (FeCN<sub>bridge</sub>), 169.1 (FeCN<sub>terminal</sub>), 169.0 (FeCN<sub>terminal</sub>), 161.9 (NC), 152.0 (C<sub>q-N=N</sub>), 150.3 (C<sub>q-N=N</sub>), 132.1 (C<sub>q</sub>-NCFe), 127.9 (*C*<sub>ortho</sub>PhNC), 127.2 (*C*<sub>ortho</sub>PhNC), 123.9 (*C*<sub>meta</sub>PhNC), 123.6 (*C*<sub>meta</sub>PhNC). IR ( $\nu_{\text{CN}}$ ): 2133, 2065 cm<sup>-1</sup>. MS (ESI<sup>-</sup>) *m/z*: {[(NC)<sub>5</sub>Fe<sup>II</sup>CN(C<sub>6</sub>H<sub>4</sub>)-N=N-(C<sub>6</sub>H<sub>4</sub>)NC]<sup>3-</sup> + 2H<sup>+</sup>}<sup>-</sup>, 420.04 (calc. 420.04); {[(NC)<sub>5</sub>Fe<sup>II</sup>CN(C<sub>6</sub>H<sub>4</sub>)-N=N-(C<sub>6</sub>H<sub>4</sub>)NC]<sup>3-</sup> + Na<sup>+</sup> + H<sup>+</sup>}<sup>-</sup>, 442.02 (calc. 442.02); {[(NC)<sub>5</sub>Fe<sup>II</sup>CN(C<sub>6</sub>H<sub>4</sub>)-N=N-(C<sub>6</sub>H<sub>4</sub>)NC]<sup>3-</sup> + 2Na<sup>+</sup>}<sup>-</sup>, 464.00 (calc. 464.00). UV-vis [ $\lambda_{\text{max}}$ , nm ( $\epsilon$ , M<sup>-1</sup> cm<sup>-1</sup>)] (water) 323 (15 000), 308 (11 000); (methanol) 330 (11 500), 470 (5500). CV (aqueous solution, E° vs. NHE): 835 mV plus the irreversible reduction wave at -680 mV.

**Na<sub>6</sub>[(NC)<sub>5</sub>Fe<sup>II</sup>CN(C<sub>6</sub>H<sub>4</sub>)-N=N-(C<sub>6</sub>H<sub>4</sub>)NCFe<sup>II</sup>(CN)<sub>5</sub>], Fe<sup>II</sup>:iso-isoFe<sup>II</sup>.** This compound was prepared following the same procedure indicated for the Na<sub>3</sub>[(NC)<sub>5</sub>Fe<sup>II</sup>CN(C<sub>6</sub>H<sub>4</sub>)-N=N-(C<sub>5</sub>H<sub>4</sub>N)] analogue but doubling the MeOH volume due to solubility issues. From 100 mg (0.43 mmol) of CN(C<sub>6</sub>H<sub>4</sub>)-N=N-(C<sub>6</sub>H<sub>4</sub>)NC and 280 mg (0.86 mmol) of Na<sub>3</sub>[Fe<sup>II</sup>(CN)<sub>5</sub>(NH<sub>3</sub>)<sub>3</sub>].3H<sub>2</sub>O, 240 mg of the desired compound was obtained (75% yield). <sup>1</sup>H NMR (D<sub>2</sub>O, 400 MHz):  $\delta$  (*trans*) 7.98 (d, *J*<sub>HH</sub> = 8.8 Hz, 4H, H<sub>meta</sub>PhNC), 7.70 (d, *J*<sub>HH</sub> = 8.8 Hz, 4H, H<sub>ortho</sub>PhNC). <sup>1</sup>H NMR (CD<sub>3</sub>OD, 400 MHz):  $\delta$  (*trans*) 7.94 (d, *J*<sub>HH</sub> = 8.8 Hz, 4H, H<sub>meta</sub>PhNC), 7.57 (d, *J*<sub>HH</sub> = 8.7 Hz, 4H, H<sub>ortho</sub>PhNC) (*cis* after irradiation) 7.35 (d, *J*<sub>HH</sub> = 8.6 Hz, 4H, H<sub>meta</sub>PhNC), 6.90 (d, *J*<sub>HH</sub> = 8.6 Hz, 4H, H<sub>ortho</sub>PhNC). <sup>13</sup>C NMR (D<sub>2</sub>O, 100.6 MHz):  $\delta$  (*trans*) 181.8 (FeCN<sub>bridge</sub>), 169.2 (FeCN<sub>terminal</sub>), 169.1 (FeCN<sub>terminal</sub>), 150.6 (C<sub>q-N=N</sub>), 131.8 (C<sub>q</sub>-NC), 127.2 (*C*<sub>ortho</sub>PhNC), 123.7 (*C*<sub>meta</sub>PhNC). IR ( $\nu_{\text{CN}}$ ): 2131, 2064 cm<sup>-1</sup>. MS (ESI<sup>-</sup>) *m/z*: {[(NC)<sub>5</sub>Fe<sup>II</sup>CN(C<sub>6</sub>H<sub>4</sub>)-N=N-(C<sub>6</sub>H<sub>4</sub>)NC

NCFe<sup>III</sup>(NC)<sub>5</sub>]<sup>4-</sup>}<sup>4-</sup>, 150.99 (calc. 150.99); {[(NC)<sub>5</sub>Fe<sup>III</sup>CN(C<sub>6</sub>H<sub>4</sub>)-N=N-(C<sub>6</sub>H<sub>4</sub>)NCFe<sup>III</sup>(CN)<sub>5</sub>]<sup>4-</sup> + H<sup>+</sup>}<sup>3-</sup>, 201.66 (calc. 201.66); {[(NC)<sub>5</sub>Fe<sup>III</sup>CN(C<sub>6</sub>H<sub>4</sub>)-N=N-(C<sub>6</sub>H<sub>4</sub>)NCFe<sup>III</sup>(CN)<sub>5</sub>]<sup>4-</sup> + Na<sup>+</sup>}<sup>3-</sup>, 208.99 (calc. 208.99). UV-vis [ $\lambda_{\text{max}}$ , nm ( $\epsilon$ , M<sup>-1</sup> cm<sup>-1</sup>)] (water) 320 (16 900), 435 (16 000); (methanol) 325 (16 000), 475 (15 000). CV (aqueous solution, E° vs. NHE): 840, 1008 mV plus the irreversible reduction wave at -680 mV.

**Na<sub>6</sub>[(NC)<sub>5</sub>Fe<sup>II</sup>CN(C<sub>6</sub>H<sub>4</sub>)-N=N-(C<sub>5</sub>H<sub>4</sub>N)Fe<sup>II</sup>(CN)<sub>5</sub>], Fe<sup>II</sup>:py-isoFe<sup>II</sup>.** 100 mg (0.2 mmol) of Na<sub>3</sub>[(NC)<sub>5</sub>Fe<sup>II</sup>CN(C<sub>6</sub>H<sub>4</sub>)-N=N-(C<sub>5</sub>H<sub>4</sub>N)] was dissolved in a purged 100 mL MeOH and 0.5 mL H<sub>2</sub>O mixture in a Schlenk tube. After complete dissolution, 65 mg (0.2 mmol) of solid Na<sub>3</sub>[Fe<sup>II</sup>(CN)<sub>5</sub>(NH<sub>3</sub>)<sub>3</sub>].3H<sub>2</sub>O was added and the mixture was left stirring for 30 min, protected from light. The resulting solution was dried to obtain the desired compound as a deep brown solid (130 mg, 90% yield). <sup>1</sup>H NMR (D<sub>2</sub>O, 500 MHz):  $\delta$  (*trans*) 9.18 (d, *J*<sub>HH</sub> = 6.9 Hz, 2H, H <sub>$\alpha$</sub> -py), 8.02 (d, *J*<sub>HH</sub> = 8.8 Hz, 2H, H<sub>meta</sub>PhNC), 7.70 (d, *J*<sub>HH</sub> = 8.8 Hz, 2H, H<sub>ortho</sub>PhNC), 7.54 (d, *J*<sub>HH</sub> = 6.9 Hz, 2H, H <sub>$\beta$</sub> -py). <sup>1</sup>H NMR (CD<sub>3</sub>OD, 400 MHz)  $\delta$  9.50 (d, *J*<sub>HH</sub> = 5.3 Hz, 2H, H <sub>$\alpha$</sub> -py), 8.00 (d, *J*<sub>HH</sub> = 8.3 Hz, 2H, H<sub>meta</sub>PhNC), 7.60 (d, *J*<sub>HH</sub> = 8.5 Hz, 2H, H<sub>ortho</sub>PhNC), 7.43 (d, *J*<sub>HH</sub> = 6.0 Hz, 2H, H <sub>$\beta$</sub> -py). <sup>13</sup>C NMR (D<sub>2</sub>O, 100.6 MHz):  $\delta$  (*trans*) 185.3 (FeCN<sub>bridge</sub>), 182.5 (FeCN<sub>Fe-py</sub>), 171.8 (FeCN<sub>terminal</sub>), 161.3 (C <sub>$\alpha$</sub> -py), 159.1 (C<sub>q-N=N</sub>), 153.4 (C<sub>q-N=N</sub>), 135.5 (C<sub>q</sub>-NC), 130.1 (*C*<sub>ortho</sub>PhNC), 127.2 (*C*<sub>meta</sub>PhNC), 117.9 (C <sub>$\beta$</sub> -py). IR ( $\nu_{\text{CN}}$ ): 2131, 2059 cm<sup>-1</sup>. MS (ESI<sup>+</sup>) *m/z*: {[(NC)<sub>5</sub>Fe<sup>II</sup>CN(C<sub>6</sub>H<sub>4</sub>)-N=N-(C<sub>5</sub>H<sub>4</sub>N)Fe<sup>III</sup>(NC)<sub>5</sub>]<sup>5-</sup> + 4Na<sup>+</sup>}<sup>-</sup>, 671.92 (calc. 671.93). CV (aqueous solution, E° vs. NHE): 480 and 840 mV plus the irreversible reduction wave at -570 mV.

## Conflicts of interest

There are no conflicts to declare.

## Acknowledgements

The financial support from the Spanish Ministerio de Ciencia e Innovación (PID2019-107006GB-C21) is acknowledged.

## References

- 1 G. S. Hartley, *Nature*, 1937, **140**, 281–281.
- 2 H. M. D. Bandara and S. C. Burdette, *Chem. Soc. Rev.*, 2012, **41**, 1809–1825.
- 3 Z. Zhang, W. Wang, M. O'Hagan, J. Dai, J. Zhang and H. Tian, *Angew. Chem., Int. Ed.*, 2022, **61**, e202205758.
- 4 A. K. Bartholomew, I. B. Stone, M. L. Steigerwald, T. H. Lambert and X. Roy, *J. Am. Chem. Soc.*, 2022, **144**, 16773–16777.
- 5 J. Garcia-Amoros, S. Nonell and D. Velasco, *Chem. Commun.*, 2012, **48**, 3421–3423.
- 6 J. Garcia-Amorós, M. Díaz-Lobo, S. Nonell and D. Velasco, *Angew. Chem., Int. Ed.*, 2012, **51**, 12820–12823.

- 7 F. Aleotti, A. Nenov, L. Salvigni, M. Bonfanti, M. M. El-Tahawy, A. Giunchi, M. Gentile, C. Spallacci, A. Ventimiglia, G. Cirillo, *et al.*, *J. Phys. Chem. A*, 2020, **124**, 9513–9523.
- 8 J. Garcia-Amorós, M. Martínez, H. Finkelman and D. Velasco, *J. Phys. Chem. B*, 2010, **114**, 1287–1293.
- 9 A. Drljaca, C. D. Hubbard, R. van Eldik, T. Asano, M. V. Basilevsky and W. J. Le Noble, *Chem. Rev.*, 1998, **98**, 2167–2289.
- 10 R. van Eldik, T. Asano and W. J. Le Noble, *Chem. Rev.*, 1989, **89**, 549–688.
- 11 J. Garcia-Amorós, M. Martínez and D. Velasco, *J. Phys. Chem. C*, 2019, **123**, 30578–30583.
- 12 J. Garcia-Amoros, G. Stopa, G. Stochel, R. van Eldik, M. Martinez and D. Velasco, *Phys. Chem. Chem. Phys.*, 2018, **20**, 1286–1292.
- 13 J. Garcia-Amoros, M. Martínez, H. Finkelmann and D. Velasco, *Phys. Chem. Chem. Phys.*, 2014, **16**, 8448–8454.
- 14 M. Han, T. Hirade and M. Hara, *New J. Chem.*, 2010, **34**, 2887–2891.
- 15 M. E. Moustafa, M. S. McCreedy and R. J. Puddephatt, *Organometallics*, 2013, **32**, 2552–2557.
- 16 M. E. Moustafa, M. S. McCreedy and R. J. Puddephatt, *Organometallics*, 2012, **31**, 6262–6269.
- 17 O. A. Blackburn and B. J. Coe, *Organometallics*, 2011, **30**, 2212–2222.
- 18 J. Long, D. Kumar, C. Deo, P. Retailleau, G. V. Dubacheva, G. Royal, J. Xie and N. Bogliotti, *Chem. – Eur. J.*, 2021, **27**, 9563–9570.
- 19 D. Barišić, I. Halasz, A. Bjelopetrović, D. Babić and M. Ćurić, *Organometallics*, 2022, **41**, 1284–1294.
- 20 M. Juribasic, K. Uzarevic, D. Gracin and M. Curic, *Chem. Commun.*, 2014, **50**, 10287–10290.
- 21 M. Bardaji, M. Barrio and P. Espinet, *Dalton Trans.*, 2011, **40**, 2570–2577.
- 22 J. Arias, M. Bardají, P. Espinet, C. L. Folcia, J. Ortega and J. Etxebarria, *Inorg. Chem.*, 2009, **48**, 6205–6210.
- 23 J. S. Park, A. M. Lifschitz, R. M. Young, J. Mendez-Arroyo, M. R. Wasielewski, C. L. Stern and C. A. Mirkin, *J. Am. Chem. Soc.*, 2013, **135**, 16988–16996.
- 24 J. Perez-Miqueo, A. Telleria, M. Munoz-Olasagasti, A. Altube, E. Garcia-Lecina, A. de Cozar and Z. Freixa, *Dalton Trans.*, 2015, **44**, 2075–2091.
- 25 A. Telleria, J. Pérez-Miqueo, A. Altube, E. García-Lecina, A. de Cózar and Z. Freixa, *Organometallics*, 2015, **34**, 5513–5529.
- 26 S. Petrovskii, A. Senchukova, V. Sizov, A. Paderina, M. Luginin, E. Abramova and E. Grachova, *Mol. Syst. Des. Eng.*, 2022, **7**, 1249–1262.
- 27 M. E. Moustafa, M. S. McCreedy, P. D. Boyle and R. J. Puddephatt, *Dalton Trans.*, 2017, **46**, 8405–8414.
- 28 Q. X. Zhou, Y. Zheng, T. J. Wang, Y. J. Chen, K. Li, C. Li, Y. J. Hou and X. S. Wang, *Chem. Commun.*, 2015, **51**, 10684–10686.
- 29 M. Lin, S. Zou, T. Li, J. Karges, Y. Chen, Y. Zhao, L. Ji and H. Chao, *Chem. Commun.*, 2022, **58**, 4324–4327.
- 30 S. S. Sun, J. A. Anspach and A. J. Lees, *Inorg. Chem.*, 2002, **41**, 1862–1869.
- 31 A. D. W. Kennedy, R. G. DiNardi, L. L. Fillbrook, W. A. Donald and J. E. Beves, *Chem. – Eur. J.*, 2022, **28**, e202104461.
- 32 O. Theilmann, W. Saak, D. Haase and R. Beckhaus, *Organometallics*, 2009, **28**, 2799–2807.
- 33 J.-Q. Wang, C.-X. Ren and G.-X. Jin, *Organometallics*, 2006, **25**, 74–81.
- 34 F. Ragon, K. Yaksi, N. F. Sciortino, G. Chastanet, J.-F. Létard, D. M. D'Alessandro, C. J. Kepert and S. M. Neville, *Aust. J. Chem.*, 2014, **67**, 1563–1573.
- 35 M. A. González, P. V. Bernhardt, M. Font-Bardia, A. Gallen, J. Jover, M. Ferrer and M. Martínez, *Inorg. Chem.*, 2021, **60**, 18407–18422.
- 36 M. A. González, A. Gallen, M. Ferrer and M. Martínez, *Inorg. Chem.*, 2020, **59**, 1582–1587.
- 37 L. Alcázar, P. V. Bernhardt, M. Ferrer, M. Font-Bardia, A. Gallen, J. Jover, M. Martínez, J. Peters and T. J. Zerk, *Inorg. Chem.*, 2018, **57**, 8465–8475.
- 38 L. Alcázar, G. Aullón, M. Ferrer and M. Martínez, *Chem. – Eur. J.*, 2016, **22**, 15227–15230.
- 39 P. V. Bernhardt, F. Bozoglian, G. González, M. Martínez, B. P. Macpherson and B. Sienra, *Inorg. Chem.*, 2006, **45**, 74–82.
- 40 P. V. Bernhardt, F. Bozoglian, B. P. Macpherson and M. Martínez, *Coord. Chem. Rev.*, 2005, **249**, 1902–1916.
- 41 P. V. Bernhardt, M. Martínez and C. Rodríguez, *Eur. J. Inorg. Chem.*, 2010, 5621–5629.
- 42 P. V. Bernhardt, M. Martínez and C. Rodríguez, *Inorg. Chem.*, 2009, **48**, 4787–4797.
- 43 M. Ferrer, A. Gallen, A. Gutiérrez, M. Martínez, E. Ruiz, Y. Lorenz and M. Engeser, *Chem. – Eur. J.*, 2020, **26**, 7847–7860.
- 44 J. Glatz, J.-R. Jiménez, L. Godeffroy, H. J. von Bardeleben, L. Fillaud, E. Maisonhaute, Y. Li, L.-M. Chamoreau and R. Lescouezec, *J. Am. Chem. Soc.*, 2022, **144**, 10888–10901.
- 45 A. Gallen, J. Jover, M. Ferrer and M. Martínez, *Inorg. Chim. Acta*, 2023, **545**, 121282.
- 46 N. Peor, R. Sfez and S. Yitzchaik, *J. Am. Chem. Soc.*, 2008, **130**, 4158–4165.
- 47 N. L. Wagner, K. L. Murphy, D. T. Haworth and D. W. Bennett, in *Inorganic Syntheses*, 2004, vol. 34, pp. 24–29.
- 48 I. Ugi, U. Fetzer, U. Eholzer, H. Knupfer and K. Offermann, *Angew. Chem., Int. Ed. Engl.*, 1965, **4**, 472–484.
- 49 Y. Yamamoto, H. Nakamura and J.-F. Ma, *J. Organomet. Chem.*, 2001, **640**, 10–20.
- 50 S. Schraff, Y. Sun and F. Pammer, *Macromolecules*, 2018, **51**, 5323–5335.
- 51 N. Masaru, R. Masahiro, W. Masayoshi, S. Kohei and O. Naoya, *Bull. Chem. Soc. Jpn.*, 1997, **70**, 737–744.
- 52 A strictly rotational transition state cannot be applied for this ligand, see Scheme S1.†
- 53 T. Asano, T. Okada, S. Shinkai, K. Shigematsu, Y. Kusano and O. Manabe, *J. Am. Chem. Soc.*, 1981, **103**, 5161–5165.

- 54 P. V. Bernhardt, G. K. Boschloo, F. Bozoglian, A. Hagfeldt, M. Martínez and B. Sienna, *New J. Chem.*, 2008, **32**, 705–711.
- 55 P. V. Bernhardt, F. Bozoglian, B. P. Macpherson, M. Martínez, A. E. Merbach, G. González and B. Sienna, *Inorg. Chem.*, 2004, **43**, 7187–7195.
- 56 P. V. Bernhardt, F. Bozoglian, B. P. Macpherson and M. Martínez, *Dalton Trans.*, 2004, 2582–2587.
- 57 P. V. Bernhardt, F. Bozoglian, B. P. Macpherson, M. Martínez, G. González and B. Sienna, *Eur. J. Inorg. Chem.*, 2003, 2512–2518.
- 58 H. Tobita, H. Habazaki and H. Ogino, *Bull. Chem. Soc. Jpn.*, 1987, **60**, 797.
- 59 A. G. Lippin, *Redox Mechanisms in Inorganic Chemistry*, Ellis Horwood, Chichester, 1994.
- 60 J. H. Espenson, *Chemical Kinetics and Reaction Mechanisms*, McGraw-Hill, New York, 1981.
- 61 N. G. Tsierkezos, *J. Solution Chem.*, 2007, **36**, 289–302.
- 62 M. Maeder and P. King, *ReactLab*, Jplus Consulting Pty Ltd, East Fremantle, WA, Australia, 2009.
- 63 R. van Eldik, in *Inorganic High Pressure Chemistry*, ed. R. van Eldik, Elsevier, 1986, pp. 1–68.
- 64 R. A. Binstead, A. D. Zuberbuhler and B. Jung, *SPECFIT32, 3.0.34*, Spectrum Software Associates, Marlborough, MA, USA, 2005.
- 65 *SAINT [7.68A]*, Bruker AXS Inc., 2009.
- 66 G. M. Sheldrick, *SADABS, 2008/1*, Bruker AXS Inc., 2008.
- 67 G. M. Sheldrick, *Acta Crystallogr., Sect. A: Found. Crystallogr.*, 2008, **64**, 112–122.
- 68 M. E. Olumba, H. Na, A. E. Friedman and T. S. Teets, *Inorg. Chem.*, 2021, **60**, 5898–5907.
- 69 D. J. Kenney, T. P. Flynn and J. B. Gallini, *J. Inorg. Nucl. Chem.*, 1961, **20**, 75–81.
- 70 I. Maciejowska, R. van Eldik, G. Stochel and Z. Stasicka, *Inorg. Chem.*, 1997, **36**, 5409–5412.